First multi-reactive polysaccharide-based transurf to produce potentially biocompatible dextran-covered nanocapsules

Laura Marcela Forero Ramirez, Jérôme Babin, Ariane Boudier, Caroline Gaucher, Marc Schmutz, Meriem Er-Rafik, Alain Durand, Jean-Luc Six, Cécile Nouvel

First multi-reactive polysaccharide-based transurf to produce potentially biocompatible dextran-covered nanocapsules

Laura Marcela Forero Ramirez[a], Jérôme Babin[a], Ariane Boudier[b], Caroline Gaucher[b], Marc Schmutz[c], Mériem Er-Rafik[c =], Alain Durand[a], Jean-Luc Six[a], Cécile Nouvel[a]*±

[a] Université de Lorraine, CNRS, LCPM, F-54000 Nancy, France

[b] Université de Lorraine, Cithefor EA 3452, Nancy F-54001, France

[c] Université de Strasbourg-CNRS- Institut Charles Sadron UPR22, Strasbourg, France.

± Current address Université de Lorraine, CNRS, LRGP, F-54000 Nancy, France

Correspondence to: Cécile Nouvel (E-mail: cecile.nouvel@univ-lorraine.fr)

= Current address DTU Nanolab, Technical University of Denmark, 2800 Kgs, Lyngby Denmark

Fax : 33(0) 3 83 32 29 75; Tel : 33(0) 3 72 74 38 32

Additional Supporting Information will be found in the online version of this article.

ABSTRACT

A multi-reactive polysaccharide-based transurf (acting both as macro-Chain Transfer Agent and stabilizer) was used to confine RAFT polymerization of methyl methacrylate (MMA) at the oil/water (o/w) miniemulsion interface. Dithiobenzoate groups and hydrophobic aliphatic side chains were introduced onto dextran, conferring it both transfer agent properties and ability to stabilize direct miniemulsion of MMA in the presence of a biocompatible oil, used as co-stabilizer. Because of their amphiphilic character, transurfs were initially adsorbed at the (o/w) interface and their reactive sites mediated RAFT polymerization *via* the R-group approach. PMMA-grafted dextran glycopolymers were consequently produced at the o/w interface, thus leading to dextran coverage/PMMA shell/oily core nanocapsules (NCs) as evidenced by Cryo-TEM analyses. The influence of dextran-based transurf chemistry and oil amount on MMA RAFT polymerization control was investigated. Positive preliminary results on NCs cytotoxicity suggest the potential of these objects for biomedical applications.

KEYWORDS

Polysaccharide
Nanocapsules
Transurf
Reversible Addition-Fragmentation chain Transfer (RAFT) polymerization
Miniemulsion
Poly(methyl methacrylate)

1. Introduction

Polymer nanocapsules (NCs) have attracted greater attention in recent years because of their unique properties and potential applications in the biomedical field, for instance as drug delivery systems (Mora-Huertas, Fessi, & Elaissari, 2010; Vrignaud, Benoit, & Saulnier, 2011; Poltorak, Durand, Léonard, Six, & Nouvel, 2015, Six, & Ferji, 2019). Miniemulsion polymerization is a promising technique that allows drug encapsulation and NCs production in one-pot (Steinmacher et al., 2010). To produce oily-core NCs by this technique, nanodroplets with size ranging from 50 to 500 nm are initially obtained by dispersion of a monomer/oil mixture in an aqueous phase. Nanodroplets are protected against coalescence by the presence of stabilizer and preserved from Ostwald ripening by the addition of an osmotic pressure agent (co-stabilizer), which may be the oil constituting the inner liquid core in the final NCs (Steinmacher et al., 2010; Landfester & Mailänder, 2013; Forero Ramirez et al., 2018). In such a case, oily core and polymeric shell will be formed during polymerization by means of induced-phase separation whereby polymer migrates to the droplet/water interface due to poor solubility in the oil. However, a well-defined core/shell structure can be difficult to obtain because of the strict thermodynamic and kinetic parameters involved in polymer/oil separation. Moreover, stabilizers are usually physically adsorbed at NCs surface and can be easily removed or replaced by surface-active molecules present in physiological media, which may thus affect the colloidal stability or enhance unwanted immune responses.

To overcome all the above limitations, some authors reported the combination of mono-reactive amphiphilic copolymers as miniemulsion stabilizers with Reversible-Deactivation Radical Polymerizations (RDRP) such as Atom Transfer Radical Polymerization (ATRP) or Reversible Addition-Fragmentation chain Transfer (RAFT) polymerization to confine polymerization at the oil/water interface. While keeping their role as stabilizers, these copolymers acted either as mono-reactive inisurfs (initiators and stabilizers) (Li,

67 Matyjaszewski, Albrecht, & Möller, 2009; Li, Yoon, & Matyjaszewski, 2010; Tian et al.,
68 2015) or transurfs (transfer agents and stabilizers) (Luo & Gu, 2007; Lu, Luo, & Li, 2010; Yu,
69 Zhang, Zhan, & Chen, 2012). This strategy was shown to offer several advantages. Firstly,
70 polymer chains grow directly at, or in the proximity of the interface thus allowing formation
71 of polymeric shell at the droplet periphery. Secondly, the stabilizer provides a permanent
72 hydrophilic covalently-linked coverage in the final NCs. Thirdly, the use of ATRP or RAFT
73 polymerization offers the possibility of precise control of macromolecular parameters of the
74 polymeric shell. With similar objectives, our team recently reported the first multi-reactive
75 dextran-based inisurf used in ATRP polymerization of butyl acrylate (Wu et al., 2015) and of
76 methyl methacrylate (MMA) (Forero Ramirez et al., 2018). In such cases, grafted dextran-
77 based copolymers were synthesized leading to nanoparticles (NPs) with covalently-anchored
78 hydrophilic dextran coverage. This coverage is expected to enhance NPs biocompatibility as
79 well as to ensure their colloidal stability and stealthiness, while offering the opportunity to
80 further functionalize their surface. Nevertheless, this ATRP process requires additional
81 purification steps to remove remaining copper catalysts after polymerization. We herein
82 hypothesize that switching ATRP to RAFT polymerization (Scheme 1) will overcome this
83 issue and will lead to the production of more suitable NCs for biomedical applications. This
84 new approach required the synthesis of a novel dextran derivative (transurf) carrying
85 hydrophobic and chain transfer agent (CTA) groups and acting as stabilizer and macro-CTA
86 during the miniemulsion process. To the best of our knowledge, it is the first time that RAFT
87 polymerization has been performed in a miniemulsion using a multi-reactive macro-CTA and
88 the above described dextran-based transurf is the second example thereof. In fact, one mono-
89 reactive dextran-based macro-CTA was previously reported for vinyl acetate polymerization
90 in emulsion, but the transurf was only formed during the polymerization process (Bernard,
91 Save, Arathoon, & Charleux, 2008). Moreover, among all the works dealing with the use of

transurfs in miniemulsion polymerization, the production of oily-core NCs is scarcely related, and the preparation of PMMA-shell NCs has never been approached, which contributes to the originality of the present work.

Herein, we hypothesize that using a dextran-based multi-reactive transurf can help to produce oily-core/PMMA shell NCs by RAFT interfacial miniemulsion polymerization Transurfs were first designed with a precise control of hydrophobic and CTA groups numbers to provide convenient stabilizing and transfer agent properties. After model studies on MMA polymerization, RAFT polymerization of MMA in miniemulsion was carried out using such dextran-based transurfs: polymerization kinetics, molar mass control and CTA groups' efficiency were studied. Detailed characterization of NCs in terms of size distribution, amount of dextran at the surface, morphology and cytotoxicity were performed to prove the formation of oily-core NCs, usable as platform for drug delivery.

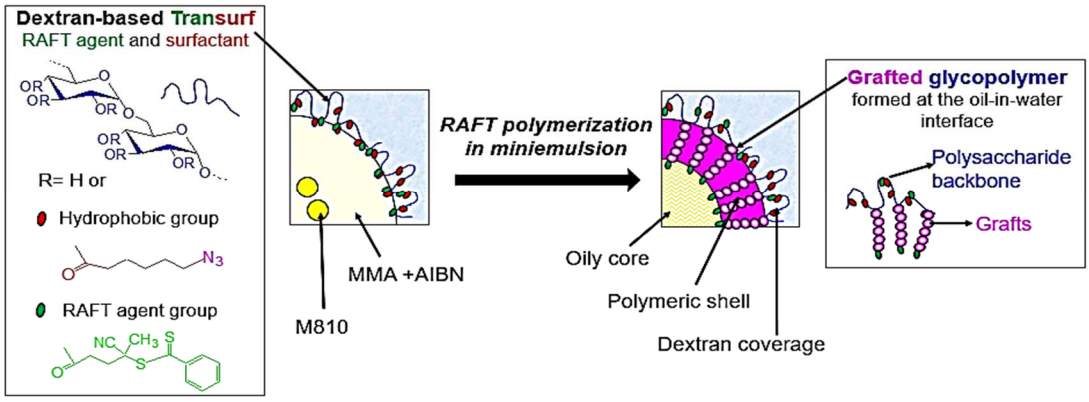

Scheme 1. Synthesis of dextran-covered oily-core NCs by MMA RAFT polymerization in miniemulsion

2. Materials and methods

2.1 Materials

Dextran T40 ($\bar{M}_n$= 26 000 g/mol, Đ = 1.3; values determined by size exclusion chromatography coupled to a multi-angle laser light scattering detector (SEC-MALLS) in DMSO/$NaNO_3$ (0,1 M)) was purchased from Aldrich. Produced from *Leuconostoc mesenteroides* B 512-F, it was having very low branching (< 5% as given by the furnisher). Consequently, it could be considered as linear. MMA (99% Aldrich) was vacuum distilled from CaH_2. 2,2-Azobis(isobutyronitrile) (AIBN, 99%, Aldrich) was purified by recrystallization from methanol. All those were used without further purification: N-(3-dimethylaminopropyl)-N′-ethylcarbodiimide hydrochloride (EDC, 99%, ABCR), 4-(dimethylamino)pyridine (DMAP, 99%, Aldrich), carbonyldiimidazole (CDI, 99%, Aldrich), 2-cyanoprop-2-yl dithiobenzoate (CPDB, >97%, Aldrich), 4-cyanopentanoic acid dithiobenzoate (CPADB, >97%, Aldrich). Miglyol®810 (M810, d = 0.94 g/cm^3, viscosity = 28 mPa.s at 20°C, water content = 0.02 wt%) was a gift from CREMER Oleo GmbH & Co. Division. M810 belonged to triacylglycerols (also called triglycerides) and was made from a mixture of saturated fatty acids (mainly caprylic acid -69.3 wt%- and capric acid -30.1 wt%), giving it a log P value of 10.2 as evaluated by group contribution methods (Ramirez, Babin, Durand, Six, & Nouvel, 2015).

2.2 Transurf synthesis

The transurf was synthesized in two steps. In the first step, the attachment of azide end-functionalized side chains onto dextran was performed in DMSO by reaction of 6-azidohexanoic acid activated with carbonyldiimidazole as previously described leading to $DexN_3$-$\boldsymbol{\tau}$ derivatives (Laville et al., 2013). In the second step, introduction of dithiobenzoate CTA groups was performed using classic EDC/DMAP catalyzed esterification and $DexN_3$-$\boldsymbol{\tau}$CTA$\boldsymbol{\gamma}$ transurfs were obtained (see Supporting Information). $\boldsymbol{\tau}$ and $\boldsymbol{\gamma}$ correspond to the

number of N_3-end alkyl chains (N_3) and dithiobenzoate CTA groups per 100 glucopyranosic units, respectively, (i. e. Substitution Degrees) and were estimated by ^{1}H NMR in DMSO-*d*$_6$ using equations 1 and 2 (Figure 1). A_{N_3}corresponds to the area of 6 methylene protons of alkyl chains (1.2 to 1.7 ppm), A_R is the area of the 5 aromatic protons of dithiobenzoate groups (7.4 to 8.1 ppm) and A_{UG} (4.3 to 5.2 ppm) corresponds globally to 4 protons per glucopyranosic unit, whatever the modification yield. The chemical shift of protons "f" was equal to 3.3 ppm, according the ^{1}H NMR spectrum of the 6-azidohexanoic acid in DMSO-d$_6$ (not shown).

$$\tau = \frac{A_{N_3}/6}{A_{UG}/4} \times 100 \qquad (1)$$

$$\gamma = \frac{A_R/5}{A_{UG}/4} \times 100 \qquad (2)$$

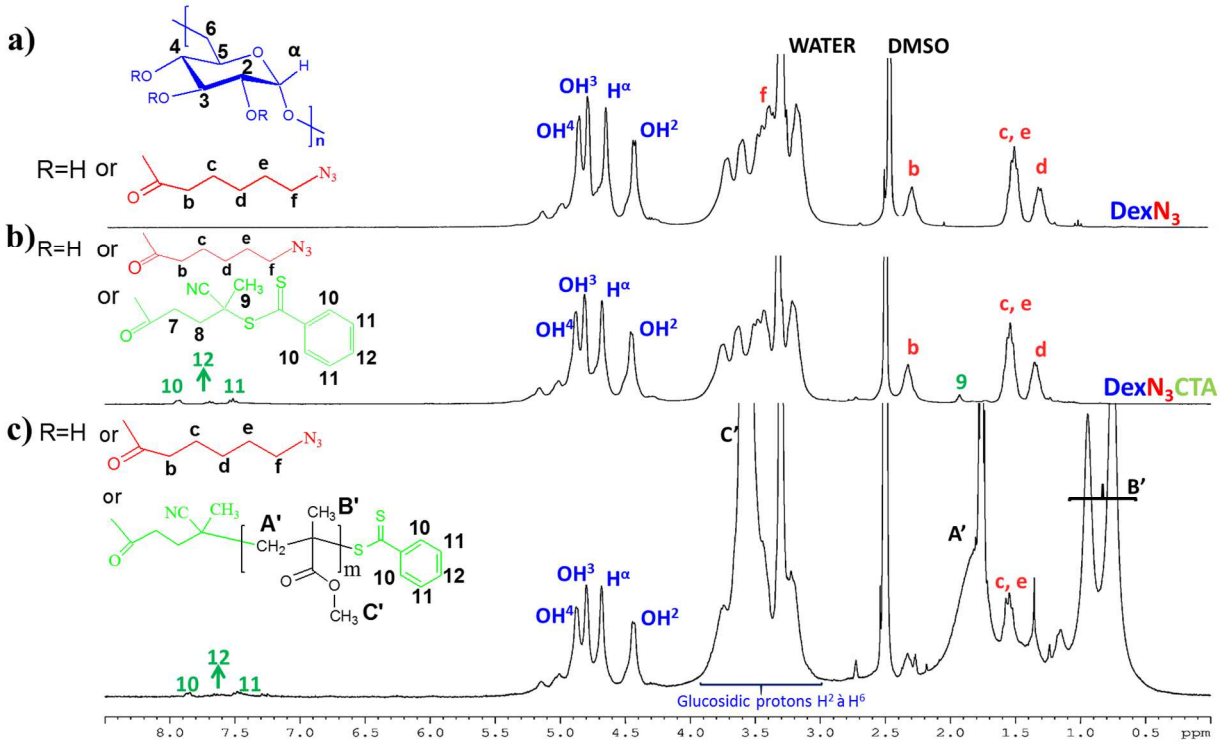

Figure 1. ^{1}H NMR spectra (DMSO-*d*$_6$) of a) DexN$_{3\text{-}20}$, b) DexN$_{3\text{-}20}$CTA$_{3.7}$ and c) DexN$_{3\text{-}20}$-g-$1.8PMMA_{7800}$.

146 *2.3 RAFT polymerization of MMA in miniemulsion*

147 Typical experimental conditions were as follows: [DexN_3-τCTAγ]$_0$ = 10 g/L, DexN_3-
148 τCTAγ /organic phase (MMA + M810) was varied from 13 to 36 wt% and M810/MMA from
149 10 to 50 vol.%. [CTA groups]$_0$/[AIBN]$_0$ molar ratio was fixed to 3. For example, in case of
150 Dex$N_{3\text{-}20}$CTA$_{3.7}$ transurf and M810/MMA = 10 vol.% (Run 1, Table 1), Dex$N_{3\text{-}20}$CTA$_{3.7}$/organic phase (MMA + M810) was 13.2 wt%. 150 mg of Dex$N_{3\text{-}20}$CTA$_{3.7}$ were
152 dissolved in 15 mL of MilliQ water. The organic phase was composed of 1.1 mL (10.3 mmol)
153 of MMA, 110 µL of M810 and 1.3 mg (7.9×10^{-3} mmol) of AIBN. The aqueous phase was
154 poured into this organic phase and the mixture was sonicated in an ice bath during 2 min
155 (51% amplitude (power 46 W), pulsed mode) using a Vibracell 600W (Sonics & Materials,
156 Dantbury, CT). Droplets size of the resulting miniemulsion was measured immediately after
157 sonication. The miniemulsion was then transferred to a Schlenk tube covered with a 3-way
158 stopcock and purged with a little nitrogen flow during 45 min at 10 °C. The reactor was then
159 immersed in a thermostatted oil bath at 80 °C to start polymerization. To follow reaction
160 kinetics and evolution of molar masses and particles size, the resulting suspensions were
161 divided in three parts. The first one was kept apart for size measurements. The second one
162 was used to determine monomer conversion (x) by a gravimetric method after vacuum drying
163 for 24 hours. NCs were washed twice with THF then dried to obtain the grafted
164 glycopolymers named DexN_3-τ-g-$nPMMA_{\bar{M}_n}$, where n is the number of PMMA grafts
165 (having an average molecular weight equal to $\bar{M}_n$) per 100 glucopyranosic units, respectively.
166 In order to study PMMA grafts, the dextran backbone of such glycopolymers was completely
167 degraded under basic conditions as previously reported (Dupayage, Save, Dellacherie,
168 Nouvel, & Six, 2008). The uncoupled PMMA grafts were analyzed by ^{1}H NMR in DMSO-d_6
169 to verify the absence of dextran backbone. Their molar masses were then characterized by
170 SEC-MALLS in THF. The remaining suspension was centrifuged. Recovered NCs were

washed twice and dispersed in deionized water for biological tests, whereas the floating was analyzed by anthrone titration (Wu et al., 2015) to estimate the quantity of $DexN_3$-τCTAγ remaining in aqueous solution. By difference with the initially introduced amount, one can estimate the quantity of dextran derivative adsorbed at the NC surface.

2.4 Characterization

^{1}H NMR and 2D DOSY ^{1}H NMR spectra were recorded on a Bruker Avance 300 apparatus (30,013 MHz, 25 ◦C) in DMSO-d_6. 1024 Scans were recorded.

Droplet and NCs sizes were measured by using a Laser Diffraction Particle Size Analyzer (Mastersizer 2000 Malvern Instruments). Washed NCs suspension (8 wt% solid content) was diluted by a factor of 200 and NCs morphology was observed by cryo-Transmission Electron Microscopy (cryo-TEM) as reported (Forero Ramirez et al., 2018).

SEC-MALLS analyses of PMMA chains were performed in THF at 40°C. Refractive index increment (dn/dc) of 0.087 mL.g^{-1} was used (See Supporting Information).

NCs cytocompatibility was evaluated on rat vascular smooth muscle cell line (A-10, ATCC_ CRL-1476™) (See Supporting Information).

3. Results and discussion

3.1 $DexN_3$-$\boldsymbol{\tau}$CTA$\boldsymbol{\gamma}$ transurf

To the best of our knowledge, relatively few examples of polysaccharides bearing RAFT functionality have been described in the literature and only 4 examples were based on dextran. One xanthate-end functionalized dextran RAFT agent was prepared by click chemistry (Bernard et al., 2008) and three multi-reactive dextran-based macro-CTA were obtained by

esterification (Duong et al., 2012; Ferji, Venturini, Cleymand, Chassenieux, & Six, 2018, Karmakar et al., 2018). Nevertheless none of them was also used as stabilizer in miniemulsion polymerization.

Herein, the first multi-reactive dextran-based transurf for a RAFT miniemulsion polymerization was synthesized and called DexN_3-τCTAγ, where τ and γ correspond to the number of N_3-end alkyl chains (N_3) and of dithiobenzoate CTA groups per 100 glucopyranosic units, respectively (Scheme 2a). On the one hand, N_3-end alkyl chains have been chosen as hydrophobic groups due to their efficiency to hydrophobize dextran, leading to amphiphilic DexN_3-τ dextran derivatives exhibiting surfactant properties (see Supporting Information). These derivatives have been successfully used to produce dextran-covered NPs via emulsion/evaporation (Laville et al., 2013; Poltorak et al., 2015) or nanoprecipitation (Laville et al., 2013) processes. In addition, azide functionality of such DexN_3-τ is expected to be suitable for potential post-modification of final NPs surface by click chemistry.

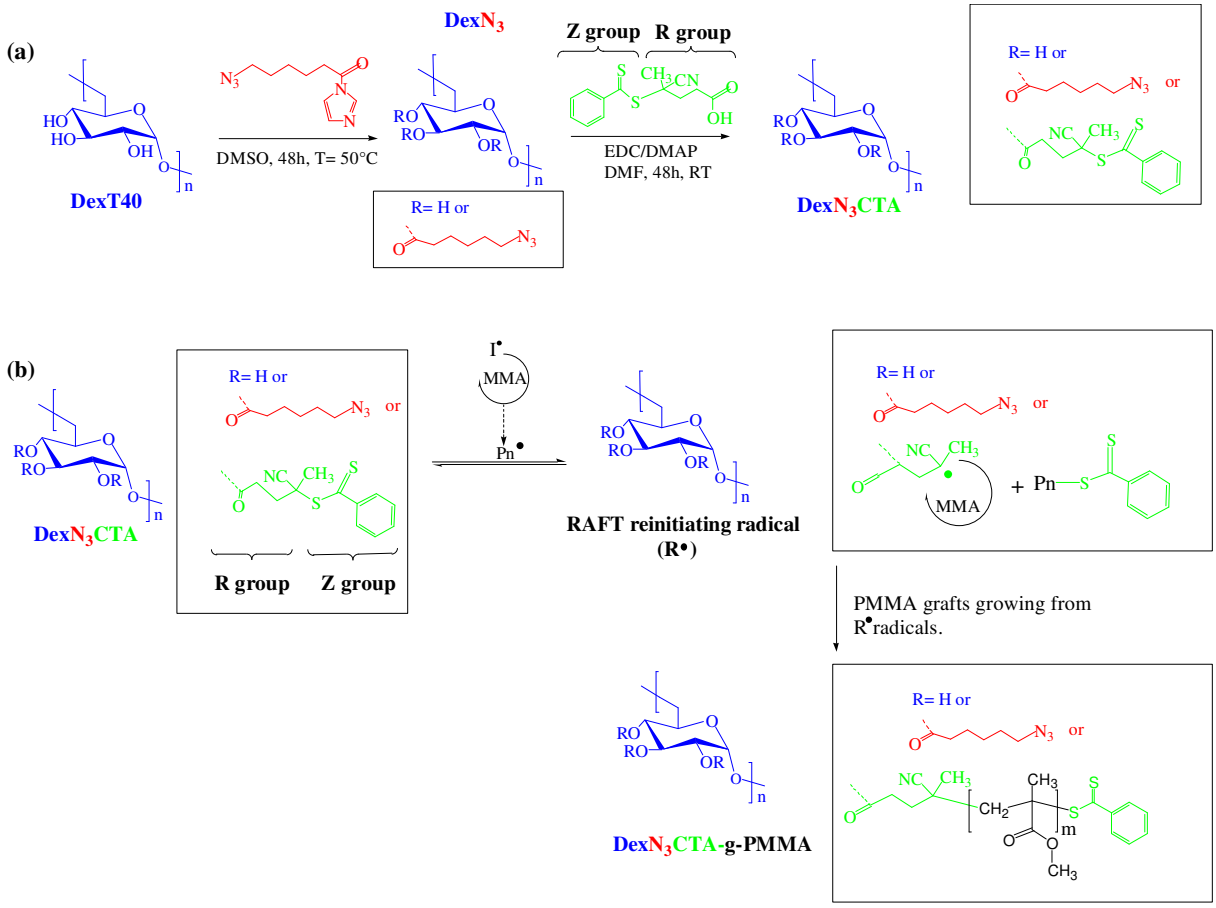

210

211 **Scheme 2.** a) Synthesis of DexN$_3$-τCTAγ transurfs. b) RAFT polymerization of MMA from
212 DexN$_3$-τCTAγ *via* the R-group approach.

213

214 On the other hand, a dithiobenzoate group bearing cyano functionality was chosen as the
215 reactive side group. Indeed, molecular CTAs having similar structure (i.e. CPDB and
216 CPADB) showed remarkable efficiency and high degree of control over MMA RAFT
217 polymerizations in homogeneous (Biasutti, Davis, Lucien, & Heuts, 2005; Johnston-Hall,
218 Stenzel, Davis, Barner-Kowollik, & Monteiro, 2007) and heterogeneous media (Yang, Luo,
219 Liu, & Li, 2009; Zhou, Ni, & Yu, 2007). CTA groups were introduced (through R-group) by
220 reacting previous DexN$_3$-τ with CPADB in the presence of EDC and a catalytic amount of
221 DMAP, resulting in DexN$_3$-τCTAγ transurfs (Scheme 2a). No degradation of the dextran
222 backbone was evidenced as attested by SEC-MALLS analysis (Table S1). The integrity of
223 grafted CTA groups was as well confirmed by ^{1}H NMR spectroscopy as characteristic protons

of both Z and R moieties clearly appeared (Figure 1b), thus ensuring its reactivity as RAFT agent. Modification degree of CTA groups (γ) could be tuned from 2 to 8% according to the experimental conditions. Those results were in quite good agreement with those previously obtained from native dextran (Duong et al., 2012).

To be used as transurfs, the designed DexN_3-τCTAγ were expected to exhibit both surfactant and transfer agent properties. To check their surface activity, steady state surface tension measurements were performed with different series of DexN_3-τ and DexN_3-τCTAγ (Figure S1). DexN_3-τ ($9 < \tau < 27$) and DexN_3-$_{20}$CTAγ transurfs (τ=20 and γ=3.7 or 7.5) were able to adsorb at the air/water interface and to reduce the surface tension of aqueous solutions. In the case of transurfs, the contribution of CTA groups to the decrease of surface tension seems less than that of N_3-end alkyl groups, at least in the range of CTA modification degree tested here, i. e. below 8%. In fact, similar curves have been observed in case of DexN_3-$_{24}$ (τ=24), DexN_3-$_{20}$CTA$_{3.7}$ (global modification degree of $\tau + \gamma \sim 24$) and DexN_3-$_{20}$CTA$_{7.5}$($\tau + \gamma \sim 27$), whereas a bigger decrease in surface tension was observed for DexN_3-$_{27}$ (τ=27). Even if CTA groups have global hydrophobic character (log P~3.4 as calculated by group contribution methods, Ramirez., Babin, Durand, Six, & Nouvel, 2015), these results could be ascribed to the presence of thiocarbonylthio and cyano functions in CTA groups in the middle of the chain, that make them less prone to segregate towards oil phase, with respect to N_3-end alkyl chains. Nevertheless, we can expect that the hydrophobic character of those CTA groups (logP~3.4) is high enough to allow direct contact of dithiobenzoate groups with the oil phase (log P ranging between 1.8 and 2.4 for initial droplet phase with M810/MMA ratio ranging from 10 to 50 vol.%), thus enabling their role as transurfs.

3.2 Miniemulsion polymerization using dextran-based transurf

After checking both the stability of the MMA miniemulsion containing M810 (a pharmaceutically acceptable triglyceride oil (Hippalgaonkar, Majumdar, & Kansara, 2010))/DexN_3-τ as co-stabilizer/stabilizer system under polymerization process, and the control of the MMA RAFT polymerization in miniemulsion using model conditions (molecular CTA + no-reactive DexN_3-τ stabilizer) (see Supporting Information), optimized conditions were applied to DexN_3-τCTAγ transurfs. Our main challenge was to evaluate the potential of the transurf to act both as oil/water interface stabilizer and macro-CTA to generate DexN_3-τ-g-$nPMMA_{\bar{M}_n}$ at the organic interface, in order to produce dextran-covered NCs with PMMA shell and M810 oily core. Thus, we first verified both the availability of CTA groups at the interface and their effective participation in RAFT polymerization. Secondly, we evaluated the effects of M810 content and transurf structure on the polymerization kinetics and control.

Table 1 summarizes all experimental recipes used in the current study, as well as the average size of initial nanodroplets and final NCs. In any case, latexes were very stable during polymerization procedure. Distribution size of the final NCs were roughly similar to the one of the initial nanodroplets, in agreement with preliminary stability assays performed with Dex$N_{3\text{-}20}$ (see Supporting Information). Depending on experimental conditions, and especially on M810 volume ratio, final solid content varied from 8 to 13 wt% in water.

Table 1. Miniemulsion polymerization of MMA at 80°C using $DexN_3$-$\tau CTA\gamma$ transurf or $DexN_{3\text{-}20}$ stabilizer with 1.1 mL of MMA. [$DexN_3$-$\tau CTA\gamma$(or $DexN_3$-τ)] = 10 g/L and $[CTA]_0/[AIBN]_0 = 3$.

Run	($DexN_3$-$\tau CTA\gamma$ or $DexN_3$-τ)/ organic phase (wt%)	$[AIBN]_0$	M810/MMA (vol.%)	Stabilizer or Transurf	$DexN_3$-$\tau CTA\gamma$ adsorbed (%) [a]	$[MMA]_0/[CTA]_0$ (or X) [b]	Nano-objects diameter (nm) [c]		Grafts number (n) [d]	Eff_{CTA} (%) [e]	F_{Homo} [f]
							After degassing	Final			
0	13.2	6.7	10	$DexN_{3\text{-}20}$	-	-	113 (1.30)	110 (1.10)	-	-	-
1	13.2	6.7	10	$DexN_{3\text{-}20}CTA_{3.7}$	94	393	102 (1.00)	102 (0.83)	1.8±0.3	48	20
2	11.6	5.7	25	$DexN_{3\text{-}20}CTA_{3.7}$	94	393	112 (1.49)	109 (1.30)	1.7±0.3	45	25
3	9.7	3.5	50	$DexN_{3\text{-}20}CTA_{3.7}$	92	402	117 (1.37)	119 (1.14)	1.8±0.3	48	25
4	11.6	11.9	25	$DexN_{3\text{-}20}CTA_{7.5}$	94	204	105 (1.31)	110 (1.30)	3.5±0.3	47	17

[a]Relative molar amount in NCs. Expressed as function of the initially introduced $DexN_3$-τCTAγ.

[b]Initial molar ratio in the organic phase, estimated with the real amount of $DexN_3$-τCTAγ at the interface evaluated in (a), and supposing that all the CTA groups were accessible for polymerization.

[c]Average nano-object diameter. Values under brackets correspond to Span (width of the distribution) calculated using $Span = (D(0.9) - D(0.1))/\ D(0.5)$. D(0.1), D(0.5) and D(0.9) were the particle diameters at 10%, 50% and 90% of the particle volume size distribution.

[d]Average number of PMMA grafts per 100 glucopyranosic units estimated from ^{1}H NMR spectrum (Figure 1c) using $n = [(4A_{A'B'}/5A_{UG}) \times \bar{M}_{n(SEC)DEX}/162)]/\bar{X}_n$. $A_{A'B'}$ and A_{UG} are the areas under peaks (A'B') and (OH^1, OH^2, OH^3 and H^α), respectively. $\bar{M}_{n(SEC)DEX}$ is the $\bar{M}_n$ of native dextran, 162 the molecular weight of one glucopyranosic unit and $\bar{X}_n$ is the average polymerization degree of PMMA grafts.

[e]Average CTA groups efficiency for transurfs estimated using $Eff_{CTA} = n/\gamma \times 100$, where n and γ are the number of grafts and CTA groups per 100 glucopyranosic units, respectively.

[f]Weight fraction of PMMA homopolymers (non-attached to dextran) with respect to the total synthesized PMMA using $F_{Homo} = \left[1 - \left[(m_{CTA}/M_{UG-CTA}) \times n \times \bar{M}_{n(SEC)grafts}\right]/(m_{MMA}x)\right] \times 100$, with m_{CTA} the mass amount of $DexN_3$-τCTAγ transurf at NCs surface, M_{UG-CTA} the molecular weight of one glucopyranosic unit of $DexN_3$-τCTAγ, n the average number of PMMA grafts per 100 glucopyranosic units evaluated in (d), $\bar{M}_{n(SEC)grafts}$ the $\bar{M}_n$ of PMMA grafts, m_{MMA} the initial mass amount of monomer and x the monomer conversion. F_{Homo} was evaluated at two different conversions and average values are given.

3.2.1 Relative amount of transurfs at nanodroplets/NCs surface.

In the early stage of RAFT polymerization, $DexN_3$-τCTAγ transurfs were located at the monomer/water interface because of their surfactant properties (Figure S1) and mediated RAFT polymerization from their multiple reactive sites. As CTA groups were attached to dextran molecules via their R moieties, re-initiating radicals (R$^\bullet$) were situated on the dextran backbone after the first addition-fragmentation step (Scheme 2b). Therefore, PMMA chains grew directly from the polysaccharide, via the R-group approach, to produce $DexN_3$-τ-g-$nPMMA_{\bar{M}_n}$ at the oil/water interface that will constitute the NCs surface/polymeric shell at the end.

For Runs 1-4 (Table 1), $[MMA]_o/[CTA]_o$ molar ratio (X) was estimated by taking into account the total amount of monomer in the system and the quantity of $DexN_3$-τCTAγ adsorbed at nanodroplets surface. This last quantity was considered in first approximation to be similar to the one at the surface of the final NCs, and was indirectly determined after NCs washing by dosage of the $DexN_3$-τCTAγ remaining in aqueous supernatant. In all cases, more than 90% of initial transurf was found to be located at the interface (Table 1). In contrast, similar analysis of PMMA latexes obtained with the model system (see Supporting Information) showed that only 60% of $DexN_{3\text{-}20}$ was present in final NCs. This result could be surprising as polymerization conditions and specially [$DexN_3$-τ]/[organic phase] weight ratio were chosen to avoid the presence of stabilizer into the aqueous phase, so as to prevent micellar or homogeneous nucleation. Nevertheless, in the model system, $DexN_{3\text{-}20}$ desorption was more prone to occur under polymerization procedure or during particle washings as the stabilizer was only physically adsorbed onto NCs surface, whereas covalent linkage between dextran backbone and PMMA chains was expected to be formed in the case of transurfs, from the first moments of the polymerization. Transurf derivatives should thus be immobilized at

NCs surface *via* their CTA groups, which would limit their desorption and explain their quantitative presence in final NCs.

3.2.2 Kinetics studies.

Figure 2 shows the first-order kinetic plots for RAFT polymerization in miniemulsion of MMA using $DexN_3$-τCTAγ transurfs. A linear relationship between $\ln([M]_o/[M]_t)$ and polymerization time was observed until at least 70% conversion, whatever the transurf or the M810 content. In addition, similar polymerization kinetics with reproducible delay period were observed when increasing M810 amount from 10 vol.% to 50 vol.% compared to MMA, while keeping $[MMA]_0/[CTA]_0$ constant (Runs 1-3). This result was quite surprising as these experiments were carried out with the same transurf, $[CTA]_o/[AIBN]_o$ ratio (equal to 3), and MMA volume.

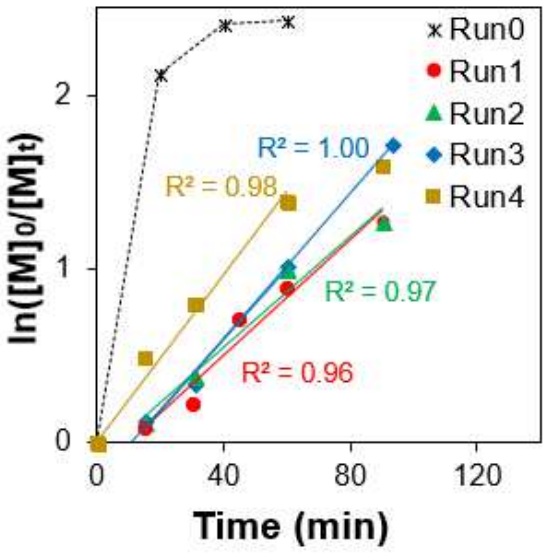

Figure 2. $Ln([M]_o/[M]_t)$ *versus* time. RAFT polymerization of MMA in miniemulsion at 80°C using $DexN_3$-τCTAγ transurfs (or $DexN_{3\text{-}20}$ stabilizer). (*) Run 0, $DexN_{3\text{-}20}$, $[CTA]_o = 0$, 10 vol.% M810 (●) Run 1, $DexN_{3\text{-}20}CTA_{3.7}$, X = 393, 10 vol.% M810 (♦) Run 2, $DexN_{3\text{-}20}CTA_{3.7}$, X = 393, 25 vol.% M810 (▲) Run 3, $DexN_{3\text{-}20}CTA_{3.7}$, X = 402, 50 vol.% M810 (■) Run 4, $DexN_{3\text{-}20}CTA_{7.5}$, X = 204, 25 vol.% M810 (see Table 1).

In such conditions, AIBN initial mass remained constant while organic phase global volume increased with the amount of M810. Polymerization rate was thus expected to slow down when increasing M810/MMA volume ratio as a result of the reduction of AIBN concentration inside nanodroplets. Nevertheless, as observed in stability studies, the increase of M810 content from 10 to 50% vol.% (which corresponded to initial organic phase volumes of 1.1 mL and 1.65 mL, respectively) resulted only in a slight increment of initial nanodroplets average size (from 102 to 117 nm) (see Supporting Information). As a consequence, the number of nanodroplets considerably increased from one experiment to another, which led to faster polymerization kinetics and, hence, offset the effect of AIBN concentration decrease, resulting in similar kinetics.

As for the model system (see Supporting Information), both studied $DexN_3$-τCTAγ transurfs appeared to slow down the miniemulsion polymerization of MMA. Indeed, $DexN_{3\text{-}20}CTA_{3.7}$ ($[AIBN]_o$ = 5.7 mM, Run 2) and $DexN_{3\text{-}20}CTA_{7.5}$ ($[AIBN]_o$ = 11.9 mM, Run 4) showed much slower kinetics when compared to a conventional radical polymerization system ($[AIBN]_o$ = 6.7 mM, Run 0). This slow down effect suggested both the availability of CTA groups at the oil/water interface and their effective involvement in growth of PMMA chains. As expected, $DexN_{3\text{-}20}CTA_{7.5}$ (Run 4) gave faster polymerization rate than $DexN_{3\text{-}20}CTA_{3.7}$ (Run 2). Since $DexN_{3\text{-}20}CTA_{7.5}$ was bearing more CTA groups, AIBN concentration was almost doubled in Run 4 with respect to Run 2 to keep constant the $[CTA]_o/[AIBN]_o$ ratio. Furthermore, no delay period was observed with $DexN_{3\text{-}20}CTA_{7.5}$ once again probably because of the higher initiator amount used in this experiment.

3.2.3 $DexN_3$-$\boldsymbol{\tau}$-g-$\boldsymbol{nPMMA_{\bar{M}_n}}$ analysis.

Attempting to confirm the covalent linkage between PMMA shell and dextran coverage of NCs, $DexN_3$-τ-g-$nPMMA_{\bar{M}_n}$ glycopolymers produced at the oil/water interface were purified

from M810 and from free PMMA homopolymers (not attached to dextran), by several washings of dried NCs with THF. These glycopolymers were also characterized with their weight fraction of PMMA (F_{PMMA}) determined by equation 3, where M_{UG-CTA} is the molecular weight of one glucopyranosic unit of $DexN_3$-τCTAγ.

$$F_{PMMA} = \frac{n\overline{M}_n}{n\overline{M}_n + 100M_{UG-CTA}} \qquad (3)$$

For copolymers produced in Runs 1 – 4, n was estimated from ^{1}H NMR spectra in DMSO-d_6 (Table 1). ^{1}H NMR spectrum of $DexN_{3\text{-}20}$-g-1.8$PMMA_{7800}$ elaborated from $DexN_{3\text{-}20}CTA_{3.7}$ (Run 3) is given in Figure 1c as example. Typical signals of dextran and PMMA parts are clearly observed, especially methyl (B', 0.5-1.0 ppm), methylene (A', 1.5-2.0 ppm) and O-CH_3 proton peaks (C', 3.6 ppm) attributed to the repeating unit of PMMA grafts, and hydroxyl and anomeric proton peaks (4.1-5.4 ppm) from the dextran backbone. Unfortunately, ester linkages between the two parts could not be proven by this method. $DexN_3$-τ-g-$nPMMA_{\overline{M}_n}$ were therefore studied by 2D Diffusion-Ordered Spectroscopy (DOSY) ^{1}H NMR (Figure 3). This technique allowed separation of the NMR signals of different species according to their diffusion coefficient. It has previously been used to discriminate between a grafted copolymer and the corresponding homopolymer mixture (Soliman, Colombeau, Nouvel, Babin, & Six, 2016). On the one hand, the 2D DOSY ^{1}H NMR spectrum of $DexN_{3\text{-}20}$-g-1.8$PMMA_{7800}$ was recorded in DMSO-d_6 (Figure 3a). As shown, a single self-diffusion coefficient was observed for all the protons from both dextran and PMMA parts (D = 4.47× 10^{-10} m^2 s^{-1}), which suggested that PMMA grew effectively from CTA groups on dextran. On the other hand, a mixture (same weight composition as for the copolymer $DexN_{3\text{-}20}$-g-1.8$PMMA_{7800}$) of the precursor $DexN_{3\text{-}20}CTA_{3.7}$ transurf and a PMMA homopolymer having roughly the same average molecular weight of PMMA grafts was also analyzed (Figure 3b). In this last case, 2D DOSY spectrum provided two different diffusion coefficients (D = 3.16 ×

10^{-11} m^2 s^{-1}and D = 1.78 × 10^{-10} m^2 s^{-1}) for transurf and PMMA, respectively. The presence of these two diffusion coefficients, compared to only one (at a different value) in case of $DexN_{3\text{-}20}$-g-1.8$PMMA_{7800}$, proved that PMMA grafts were really covalently linked to dextran backbone, resulting in a $DexN_{3}$-τ-g-$nPMMA_{\bar{M}_n}$ glycopolymer.

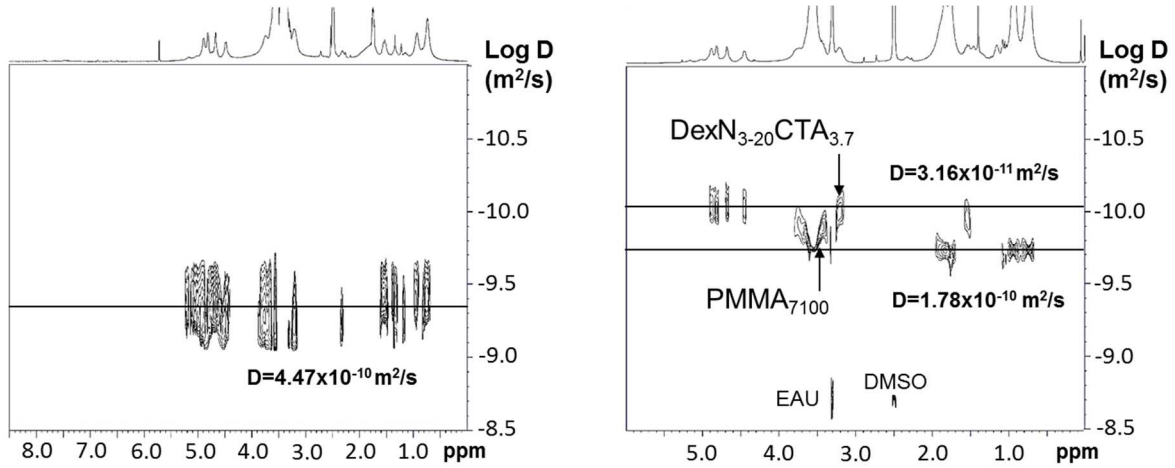

Figure 3. 2D DOSY ^{1}H NMR spectra of a) $DexN_{3\text{-}20}$-g-1.8$PMMA_{7800}$ (F_{PMMA}= 43%) obtained from Run 3 (Table 1) at 12% of conversion and b) mixture of $PMMA_{7100}$ and $DexN_{3\text{-}20}CTA_{3.7}$ (43/57; w/w).

Finally, we wanted to characterize those $DexN_{3}$-τ-g-$nPMMA_{\bar{M}_n}$ glycopolymers by SEC-MALLS. Nevertheless, it was difficult to find an appropriate solvent able to well solubilize both the hydrophilic polysaccharide and the hydrophobic PMMA parts. Despite solubility problems resulting in the appearance of numerous aggregate peaks on the SEC trace, chromatograms of purified $DexN_{3}$-τ-g-$nPMMA_{\bar{M}_n}$ (i.e. after washing with THF- Figure S6) clearly showed a shift of the molecular weight distribution toward higher molar masses in comparison with the chromatogram of the precursor transurf, which further attested to the copolymer formation. Nonetheless, accurate average molar masses were not accessible from these SEC-data due to the above-mentioned solubility issues. Non-purified $DexN_{3}$-τ-g-$nPMMA_{\bar{M}_n}$ (i.e. before THF washings) were also investigated. In comparison with chromatograms of purified glycopolymers, an additional smaller peak evolving with

conversion was detected at high elution time. This peak, disappearing after purification, was found to correspond to PMMA homopolymers (non-attached to dextran) formed during polymerization, as confirmed by ^{1}H NMR spectrum of the product extracted with THF. This observation was not a surprise. The production of a small percentage of homopolymer is inherent to the RAFT process since chains are initiated by AIBN decomposition. Thus, in addition to PMMA chains re-initiated by CTA groups and growing from the dextran backbone at the oil/water interface, there is also a small fraction of PMMA chains coming from AIBN and propagating within the organic phase. Furthermore, irreversible transfer reactions could also eventually lead to homopolymer formation. For all experiments, homopolymer fraction (F_{Homo}) was evaluated to about 20 wt% of the total produced polymer amount (Table 1), which remains quite reasonable and below the maximum amount evaluated for a $[CTA]_0/[AIBN]_0$ ratio of 3. We can expect that this relatively low fraction would not have a significant adverse impact on the desired core-shell morphology control.

3.2.4 Polymerization control and CTA groups efficiency.

In order to ascertain the degree of RAFT polymerization control, PMMA grafts were deliberately uncoupled from dextran backbone, then characterized by SEC-MALLS. Total PMMA recovery was achieved under basic conditions already proven to be harmless for PMMA grafts (Dupayage et al., 2008; Forero Ramirez et al., 2018). SEC of uncoupled PMMA chains exhibited monomodal distributions at low conversion and a clear shift toward higher molar masses with conversion (Figure 4a). For conversions above 50%, a small molecular weight shoulder was however observed suggesting a small proportion of irreversible deactivation by bimolecular termination between two PMMA grafts, or more probably between a PMMA graft and a PMMA homopolymer. When comparing polymerizations carried out with the same transurf but different M810 contents, similar SEC traces were observed at analogous conversions indicating that M810 amount has no influence

on RAFT polymerization control. Furthermore, molar mass distributions of PMMA homopolymers (unlinked to dextran) overlaid pretty well with those of PMMA grafts obtained at the same conversion (Figure S7). This showed that the exchange of thiocarbonylthio groups between grafted and free PMMA chains was quite effective to allow the control of macromolecular parameters of both types of chains. Overall these results indicated the absence of noticeable transfer or termination reactions, except a small proportion of termination by recombination of PMMA grafts (no shoulder was detected in case of homopolymers). Bimolecular termination between a PMMA graft and a PMMA homopolymer was more prone to occur at high conversion and with consequent amount of M810 in the organic phase. Actually, sufficient amount of M810 in the organic phase was expected to favor phase segregation between the oily core and the polymer shell (see 3.3), and thus, the geographic proximity between free PMMA chains (growing into the organic phase) and PMMA grafts (growing at the interface). Bimolecular termination between two PMMA grafts was less probable to happen. Furthermore, such termination would have resulted in the reticulation of the system, which was never observed in any case.

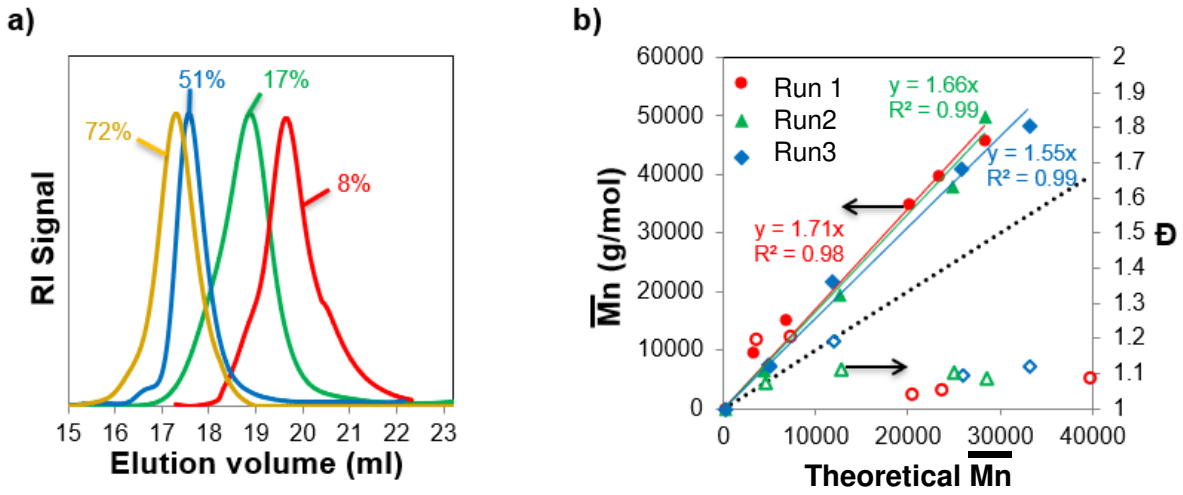

Figure 4. Evolution of a) SEC traces (Refractive Index detector) of PMMA grafts (Run 2) and b) experimental $\overline{M}_n$ (full symbols), Dispersity Đ (open symbols) *versus* conversion. Conversions are given in % on figure a). RAFT polymerization of MMA in miniemulsion at 80°C using $DexN_{3\text{-}20}CTA_{3.7}$ transurf and various amounts of M810 in the organic phase (●)

Run 1, 10 vol.% (♦) Run 2, 25 vol.% (▲) Run 3, 50 vol.%. See Table 1 for other conditions. Theoretical $\overline{M}_n$ (dotted lines) was evaluated using $\overline{M}_n = 100(x)(X)$ where *x* and 100 are the monomer conversion and the molecular weight of a PMMA unit, respectively. Curve for X = 393 is given.

The evolution of experimental $\bar{M}_n$ of PMMA grafts with conversion for Runs 1-3 is shown as a function of theoretical $\bar{M}_n$ in Figure 4b. In all cases, experimental $\bar{M}_n$ evolved linearly with conversion until 80% of conversion without appearance of noticeable transfer or termination reactions. In addition, Đ remained considerably below 1.2. All these results further attested of RAFT control during almost the whole polymerization. Experimental $\overline{M}_n$ were however much higher than the theoretical ones (calculated with the adjusted average value of X = $[MMA]_o/[CTA]_o$=393) indicating that not all CTA groups participated in the polymerization (Figure S8 for additional results of Run 4, X = 402). The comparison between the number of grafts (n) estimated from ^{1}H NMR spectra and the number of CTA groups along dextran backbone (γ) allowed us to evaluate an average efficiency of CTA groups (Eff_{CTA}) of about 48% (Table 1). Roughly half of the initial CTA groups of $DexN_3$-τCTAγ transurfs located at the interface, effectively resulted in a PMMA grafted chain. Similar lower efficiencies have been already observed for other polysaccharides bearing reactive groups when used for controlling ATRP (Dupayage et al., 2008; Ferji et al., 2015) in homogeneous media. One possible cause seemed to be the presence of intramolecular termination reactions at the very beginning of the polymerization resulting in the loss of RAFT re-initiating radicals ($R^{\bullet}$). In our case, the reaction takes place in a heterogeneous environment. So, the transurf conformation at the oil/water interface is more likely the key factor limiting the availability of some CTA groups for polymerization if they are not facing to the organic phase, which was the main challenge of this work. Finally, CTA group efficiency appeared to be the same for both $DexN_{3\text{-}20}CTA_{3.7}$ and $DexN_{3\text{-}20}CTA_{7.5}$, and remained unchanged whatever the M810/MMA volume ratio in agreement with our previous results for miniemulsion ATRP of

MMA using dextran-based inisurfs (Forero Ramirez et al., 2018). A steric hindrance effect in the vicinity of CTA groups restricting the access to C=S function does not seem to be present in the range of studied CTA modification degrees.

3.3 Nano-objects morphology

Indirect confirmation of an oily-core/polymeric shell morphology of final objects was provided by MDSC analysis. The obtained thermograms (Figure S9) showed that NCs made with 25-50 vol.% of M810 (Runs 2, 3 and 4) were effectively two-phase systems having: i) a plasticized amorphous phase of PMMA/M810 (11 / 89 w / w, T_g = 98 °C) and ii) a pure M810 liquid phase exhibiting one melting transition (T_m = - 4°C). On the contrary, nano-objects formulated with 10 vol.% of M810 (Run 1) displayed only a single glass transition event indicating a total miscibility of two components. These results were in quite agreement with our previous studies on PMMA/M810 blends miscibility as M810 was shown to plasticize PMMA until a weight fraction of 11 wt% (Forero Ramirez et al., 2018).

In order to prove NCs morphology in a direct way, final nano-objects were analyzed by Cryogenic-Transmission Electron Microscopy (cryo-TEM). Electron micrograph of NCs obtained with 25 vol.% of M810 in the organic phase (Run 2, Table 1) at 93% of conversion is shown in Figure 5. Cryo-TEM image showed the sphericity of synthesized objects as well as the average diameter determined by Laser granulometry, which varies from around 200 nm to 50 nm. A few particles are even smaller in that case the inner oily core is not clearly seen. The lack of sufficient contrast between plasticized PMMA and pure M810 phases render the visualization of the oily-core/polymeric shell structure under low dose conditions not simple. The core shell structure is best seen on small objects. On the larger objects the PMMA layer is just slightly darker than the oily core. The shell thickness is around 25 nm on all objects of run 2, Table 1. Internal liquid oil cavity was more visible for large objects after exposure to

488 the microscope electron beam since the polymeric shell was less sensitive to irradiation
489 damage (Figure S10). These observations provided direct evidence of core-shell structure
490 formation. Improved studies will be however needed to further characterize NCs morphology.

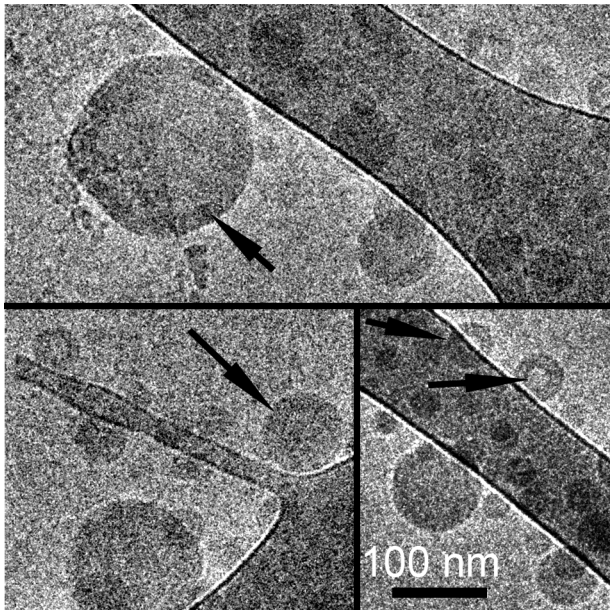

491

492 **Figure 5.** Assembly of Cryo-TEM micrographs of final NCs obtained from Run 2. The black
493 arrows point towards the shell of the particle. The scale bar is the same for each 3 images.

494

495 *3.4 Nano-objects cytocompatibility*

496 Formulated NCs are constituted of an oily liquid biocompatible M810 core, an inner shell of
497 PMMA (frequently used in implantable medical devices (Frazer, Byron, Osborne, & West,
498 2005)) and an outer shell of dextran (well-known biodegradable and bioeliminable
499 polysaccharide (Posocco et al., 2015)). In order to check the potential of these NCs for
500 intravenous drug administration, preliminary cytocompatibility studies on vascular smooth
501 muscle cells were performed *in vitro*. NCs prepared with the model system (see Supporting
502 Information), called MOD, and with transurfs (called CTA-PMMA) were both analyzed.
503 Metabolic activity of vascular cells was measured by monitoring the conversion of MTT to
504 formazan. The reduction of MTT is catalyzed by mitochondrial dehydrogenase enzymes and

505 is therefore a measure for cell viability. After 24 hours, results expressed as percentages did
506 not show any variation whatever the concentration or NCs type, when compared to the control
507 condition (no NC) (Figure 6). The MOD and CTA-PMMA NCs appeared to be
508 cytocompatible with vascular smooth muscle cells.

509

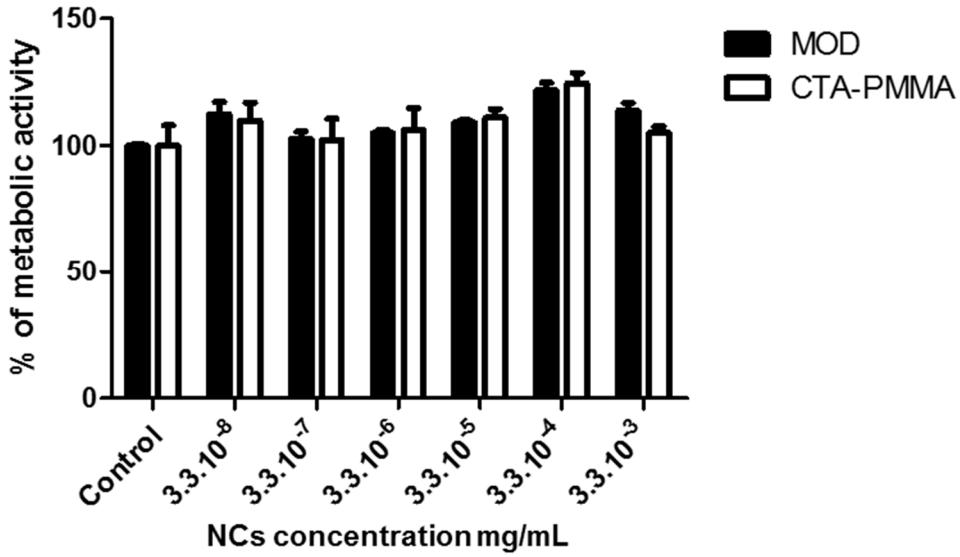

510

511 **Figure 6.** Cytocompatibility of MOD (prepared with a $[MMA]_o/[CPDB]_o$ molar ratio of 700
512 and 25 vol.% of M810 compared to MMA, see Supporting Information) or CTA-PMMA NCs
513 (Run 2, Table 1) towards rat vascular smooth muscle cells (A-10) after 24 h incubation at
514 37°C. 100% of metabolic activity (MTT assay) represents control cells incubated with PBS.
515 Results expressed as mean ± standard error of the mean, n = 3.

516

517 **4. Conclusions**

518 As stated, we designed dextran-based transurfs able to produce oily-core/PMMA shell NCs by
519 RAFT interfacial miniemulsion polymerization. The two major challenges of this work were
520 to introduce CTA functionalities onto dextran in order to synthesize a multi-reactive transurf
521 (acting both as macro-CTA and stabilizer) and to check its ability to confine RAFT
522 miniemulsion polymerization of MMA at the oil/water interface. About a half of the CTA
523 groups along dextran backbone were found to effectively initiate a PMMA grafted chain.

About 80 wt% of the total produced PMMA was effectively attached to dextran backbone. In any case, polymerization was controlled until high conversion as concluded from the analysis of uncoupled PMMA grafts deliberately removed from $DexN_3\text{-}\tau\text{-g-}nPMMA_{\overline{M}_n}$. Phase segregation between PMMA shell and M810 core was evidenced.

Overall these results highlight the value of our novel dextran-based transurf to produce dextran-covered oily-core NCs having different oil contents. Such NCs can be potentially used in drug delivery applications as indicated by preliminary *in vitro* cytotoxicity tests. Complementary biological tests, deep characterization of covalently linked dextran coverage, as well as post-functionalization of final NCs *via* the azide functions will be reported soon. The possibility of extending this method to RAFT copolymerization of MMA with a pH-responsive monomer will be also studied in the near future.

ACKNOWLEDGEMENTS

C. Nouvel and L.M Forero Ramirez acknowledge support from ANR JCJC ANR-12-JS08-0003-01 NANOCAPDEX for funding and PhD Research Fellowship, respectively.

The authors express their highest gratitude to Olivier Fabre for NMR analyzes, to Marie-Christine Grassiot for help in SEC measurements andto Isabelle Fries for cytotoxicity assays.

References

Bernard, J., Save, M., Arathoon, B., & Charleux, B. (2008). Preparation of a xanthate-terminated dextran by click chemistry: Application to the synthesis of polysaccharide-coated nanoparticles via surfactant-free ab initio emulsion polymerization of vinyl acetate. *Journal of Polymer Science Part A: Polymer Chemistry*, *46*(8), 2845–2857.

Biasutti, J. D., Davis, T. P., Lucien, F. P., & Heuts, J. P. A. (2005). Reversible addition-fragmentation chain transfer polymerization of methyl methacrylate in suspension. *Journal of Polymer Science Part A: Polymer Chemistry*, *43*(10), 2001–2012.

Duong, H. T. T., Hughes, F., Sagnella, S., Kavallaris, M., Macmillan, A., Whan, R., … Boyer, C. (2012). Functionalizing Biodegradable Dextran Scaffolds Using Living Radical Polymerization: New Versatile Nanoparticles for the Delivery of Therapeutic Molecules. *Molecular Pharmaceutics*, *9*(11), 3046–3061.

Dupayage, L., Save, M., Dellacherie, E., Nouvel, C., & Six, J.-L. (2008). PMMA-grafted dextran glycopolymers by atom transfer radical polymerization. *Journal of Polymer Science Part A: Polymer Chemistry*, *46*(23), 7606–7620.

Ferji, K., Nouvel, C., Babin, J., Li, M.-H., Gaillard, C., Nicol, E., … Six, J.-L. (2015). Polymersomes from Amphiphilic Glycopolymers Containing Polymeric Liquid Crystal Grafts. *ACS Macro Letters*, *4*(10), 1119–1122.

Ferji, K., Venturini, P., Cleymand, F., Chassenieux, C., & Six, J.-L. (2018). *In situ* glyco-nanostructure formulation *via* photo-polymerization induced self-assembly. *Polymer Chemistry*, *9*(21), 2868–2872.

Forero Ramirez, L.M., Babin, J., Schmutz, M., Durand, A., Six, J.-L., & Nouvel, C. (2018). Multi-reactive surfactant and miniemulsion Atom Transfer Radical Polymerization: An elegant controlled one-step way to obtain dextran-covered nanocapsules. *European Polymer Journal*, *109*, 317–325.

Frazer, R. Q., Byron, R. T., Osborne, P. B., & West, K. P. (2005). PMMA: An Essential Material in Medicine and Dentistry. *Journal of Long-Term Effects of Medical Implants*, *15*(6), 629–639.

Hippalgaonkar, K., Majumdar, S., & Kansara, V. (2010). Injectable Lipid Emulsions—Advancements, Opportunities and Challenges. *AAPS PharmSciTech*, *11*(4), 1526–1540.

Johnston-Hall, G., Stenzel, M. H., Davis, T. P., Barner-Kowollik, C., & Monteiro, M. J. (2007). Chain Length Dependent Termination Rate Coefficients of Methyl Methacrylate (MMA) in the Gel Regime: Accessing $k_t^{i,i}$ Using Reversible Addition-Fragmentation Chain Transfer (RAFT) Polymerization. *Macromolecules*, *40*(8), 2730–2736.

Karmakar, P. D., Seesala, V. S., Pal, A., Dhara, S. , Chatterjee, S., & Pal, S. (2018). Synthesis of RAFT-Mediated Amphiphilic Graft Copolymeric Micelle Using Dextran and Poly (Oleic Acid) toward Oral Delivery of Nifedipine. *Journal of Polymer Science Part A: Polymer Chemistry*, *56*(20), 2354–2363.

Landfester, K., & Mailänder, V. (2013). Nanocapsules with specific targeting and release properties using miniemulsion polymerization. *Expert Opinion on Drug Delivery*, *10*(5), 593–609.

Laville, M., Babin, J., Londono, I., Legros, M., Nouvel, C., Durand, A., … Six, J.-L. (2013). Polysaccharide-covered nanoparticles with improved shell stability using click-chemistry strategies. *Carbohydrate Polymers*, *93*(2), 537–546.

Li, W., Matyjaszewski, K., Albrecht, K., & Möller, M. (2009). Reactive Surfactants for Polymeric Nanocapsules via Interfacially Confined Miniemulsion ATRP. *Macromolecules*, *42*(21), 8228–8233.

Li, W., Yoon, J. A., & Matyjaszewski, K. (2010). Dual-Reactive Surfactant Used for Synthesis of Functional Nanocapsules in Miniemulsion. *Journal of the American Chemical Society*, *132*(23), 7823–7825.

Lu, F., Luo, Y., & Li, B. (2010). pH Effects on the Synthesis of Nanocapsules via Interfacial Miniemulsion Polymerization Mediated by Amphiphilic RAFT Agent with the R Group of Poly(methyl acrylic acid- *ran* -styrene). *Industrial & Engineering Chemistry Research*, *49*(5), 2206–2212.

Luo, Y., & Gu, H. (2007). Nanoencapsulation via interfacially confined reversible addition fragmentation transfer (RAFT) miniemulsion polymerization. *Polymer*, *48*(11), 3262–3272.

Mora-Huertas, C. E., Fessi, H., & Elaissari, A. (2010). Polymer-based nanocapsules for drug delivery. *International Journal of Pharmaceutics*, *385*(1–2), 113–142.

Poltorak, K., Durand, A., Léonard, M., Six, J.-L., & Nouvel, C. (2015). Interfacial click chemistry for improving both dextran shell density and stability of biocompatible nanocapsules. *Colloids and Surfaces A: Physicochemical and Engineering Aspects*, *483*, 8–17.

Posocco, B., Dreussi, E., de Santa, J., Toffoli, G., Abrami, M., Musiani, F., … Dapas, B. (2015). Polysaccharides for the Delivery of Antitumor Drugs. *Materials*, *8*(5), 2569–2615.

Ramirez, L.M., Babin, J., Durand, A., Six, J.-L., & Nouvel, C. (2015). Biocompatible dextran-covered nanoparticles produced by Activator Generated by Electron Transfer Atom Transfer Radical Polymerization in miniemulsion. *Colloids Surf., A*, *486*, 60-68.

Six, J.-L. & Ferji, K (2019). *Polymerization induced self-assembly: an opportunity toward the self-assembly of polysaccharide-containing copolymers into high-order morphologies*. *Polymer Chemistry*, *10*(1), 45–53.

Soliman, S. M. A., Colombeau, L., Nouvel, C., Babin, J., & Six, J.-L. (2016). Amphiphilic photosensitive dextran-g-poly(o-nitrobenzyl acrylate) glycopolymers. *Carbohydrate Polymers*, *136*, 598–608.

Steinmacher, F. R., Bernardy, N., Moretto, J. B., Barcelos, E. I., Araújo, P. H. H., & Sayer, C. (2010). Kinetics of MMA and VAc Miniemulsion Polymerizations Using Miglyol and Castor Oil as Hydrophobe and Liquid Core. *Chemical Engineering & Technology*, *33*(11), 1877–1887.

Tian, K., Zeng, J., Zhao, X., Liu, L., Jia, X., & Liu, P. (2015). Synthesis of multi-functional nanocapsules via interfacial AGET ATRP in miniemulsion for tumor micro-environment responsive drug delivery. *Colloids and Surfaces B: Biointerfaces*, *134*, 188–195.

Vrignaud, S., Benoit, J.-P., & Saulnier, P. (2011). Strategies for the nanoencapsulation of hydrophilic molecules in polymer-based nanoparticles. *Biomaterials*, *32*(33), 8593–8604.

Wu, M., Forero Ramirez, L. M., Rodriguez Lozano, A., Quémener, D., Babin, J., Durand, A., Marie, E. Six, J.-L & Nouvel, C. (2015). First multi-reactive dextran-based inisurf for atom transfer radical polymerization in miniemulsion. *Carbohydrate Polymers*, *130*, 141–148.

Yang, L., Luo, Y., Liu, X., & Li, B. (2009). RAFT miniemulsion polymerization of methyl methacrylate. *Polymer*, *50*(18), 4334–4342.

Yu, Y., Zhang, Q., Zhan, X., & Chen, F. (2012). Comparison of styrene reversible addition-fragmentation chain-transfer polymerization in a miniemulsion system stabilized by ammonlysis poly(styrene-alt-maleic anhydride) and sodium dodecyl sulfate. *Journal of Applied Polymer Science*, *124*(5), 4249–4258.

Zhou, X., Ni, P., & Yu, Z. (2007). Comparison of RAFT polymerization of methyl methacrylate in conventional emulsion and miniemulsion systems. *Polymer*, *48*(21), 6262–6271.